Journal of Applied Electrochemistry **29**: 551–560, 1999.

Comparative study of nanocrystalline Ti_2RuFe and Ti_2RuFeO_2 electrocatalysts for hydrogen evolution in long-term chlorate electrolysis conditions

L. ROUÉ[1], É. IRISSOU[1], A. BERCIER[1], S. BOUARICHA[1], M. BLOUIN[1], D. GUAY[1]*, S. BOILY[2], J. HUOT[2] and R. SCHULZ[2]

[1]*INRS-Énergie et Matériaux, 1650 Boulevard Lionel-Boulet, C.P. 1020, Varennes, Québec, Canada, J3X 1S2;* [2]*Technologies Émergentes de Production et de Stockage, Institut de Recherche d'Hydro-Québec, Varennes, Québec, Canada*

*(*author for correspondence)*

Received 6 May 1998; accepted in revised form 15 September 1998

Key words: ball-milling, electrocatalyst, hydrogen evolution, nanocrystalline alloy, sodium chlorate

Abstract

Ti_2RuFe and Ti_2RuFeO_2 nanocrystalline alloys were prepared by high energy ball-milling and used as cathodes for the hydrogen evolution reaction (HER) in the process of sodium chlorate synthesis. Ti_2RuFe is almost single phase with the B2 structure. In contrast, Ti_2RuFeO_2 is made of a mixture of Ti_2RuFe and TiO_x phases. Tests in chlorate electrolysis conditions did not show any sign of degradation of Ti_2RuFeO_2 over a 300 h period, while Ti_2RuFe breaks down after less than 100 h. The degradation of Ti_2RuFe occurs because of hydrogen absorption and desorption during alternating hydrogen discharge and open-circuit conditions. Various hypotheses to explain the increase stability of the O containing alloy are considered.

1. Introduction

The first step in the formation of sodium chlorate is the anodic discharge of chloride ions, while hydrogen is evolved at the opposite electrode. From then chlorate is formed through a series of chemical reactions. In this process, approximately 50% of the production costs are associated with the consumption of electrical energy. The overall efficiency of an electrolysis cell depends on several factors [1], of which the choice of electrode materials for the anodic and cathodic reactions is of utmost importance.

Since the introduction of the dimensionally stable anode (DSA®) in the chlorate industry, not much energy saving can be gained by developing new activated anodes. DSA electrodes give very low anodic overpotential, typically 40 mV at 250 mA cm^{-2}. On the other hand, the cathodic overpotential of the steel cathodes used by some producers is about −800 mV at −250 mA cm^{-2}. This constitutes the main electrochemical energy loss in the production of sodium chlorate. The cathodic overpotential is even more negative in the case of Ti-based electrodes, although their better corrosion resistance compared to steel cathodes introduces other advantages when the process is considered as a whole. Obviously, important energy savings could be obtained by developing more efficient cathodes.

Numerous electrode materials have been developed and tested to catalyse the hydrogen discharge reaction [2]. However, to qualify a given material as a viable chlorate cathode, the following requirements must be met to some extent: (a) low H_2 evolution overpotential; (b) inactive towards hypochlorite decomposition; (c) must not interfere with selectivity of the dynamic chromium hydroxide film; (d) stable under OCP conditions in hot chlorate liquor; (e) must not hydride; (f) must withstand periodic rinse in 5–10% HCl; (g) lifetime of several years; (h) low cost; and (i) must be easy to apply on a suitable substrate. Obviously, this long list of criteria reduces considerably the potential candidates.

We have shown a few years ago that nanocrystalline alloys with excellent electrocatalytic properties for hydrogen discharge in basic solutions could be produced by high energy ball-milling [3]. Unfortunately, these materials (Ni–Mo–O) contain nickel and could not be accepted as a viable alternative to steel or titanium cathodes. Nevertheless, these results were showing that electrocatalysts with remarkable performances could be

obtained by mechanical alloying. This technique has been successfully applied to the synthesis of various materials for a number of different applications and the field of mechanosynthesis is now quite important in materials sciences, as demonstrated with the recently published reviews of C. Suryanarayana [4] and Koch and Whittenberger [5].

High energy mechanical alloying consists of inducing a solid state reaction between the components of a powder mixture by repeated mechanical deformations caused by ball–powder–ball and ball–powder–wall collisions. During this process, numerous structural defects which increase the inter-diffusion of elements are created. Strain is also introduced in the lattice, and as a result crystals fracture into smaller pieces. The growing interest for this technique resides in the possibility of fabricating materials with unique chemical, physical and mechanical properties.

Recently, we have shown that considerable improvement in the electrocatalytic activity for hydrogen evolution in typical chlorate electrolysis conditions can be obtained by using activated cathodes based on nanocrystalline Ti–Ru–Fe alloys prepared by ball-milling [6–11]. Indeed, a reduction of the cathodic overpotential at -250 mA cm^{-2} by about 250 mV was observed over a one hour electrolysis test [10, 11]. This represents a reduction of the cell voltage of almost 10% compared to steel cathodes.

For industrial applications, stability issues are as important as the activity of a material and the energy savings when determining a suitable electrode material. We have shown previously that the addition of O to nanocrystalline Ti–Ru–Fe alloys was essential for its long-term stability [7] and that nanocrystalline alloys based on Ti–Ru–Fe–O were promising materials for use as activated cathodes. However, the mechanisms underlying the degradation of the oxygen-free alloys are unknown. This study was undertaken to answer these questions.

There are two mechanisms that can play a role in the degradation of the O-free nanocrystalline Ti–Ru–Fe alloys: corrosion or oxidation of the electrode during open-circuit conditions and hydrogen embrittlement [12]. These mechanisms can lead to the crumbling of electrodes [13]. This paper gives a thorough comparison of the long term stability of nanocrystalline Ti_2RuFe and Ti_2RuFeO_2 electrodes in chlorate electrolysis conditions. By combining the results of electrochemical experiments with chemical and structural analyses and gas phase hydrogen absorption measurements, hypotheses to explain the degradation process of nanocrystalline Ti_2RuFe electrodes and the improvement of stability by the addition of O will be proposed.

2. Experimental details

2.1. *Preparation of nanocrystalline Ti_2RuFe and Ti_2RuFeO_2 alloys*

Pure Ti (99.5%, -325 mesh, from Aesar), Ru (99.95%, -325 mesh, from Aesar), Fe (99.9%, 100–200 mesh, from Cerac) and RuO_2 (Ru 99.95%, from Aesar) powders were used as starting materials. The ball-milling was performed with a SPEX 8000 mixer mill. Five grams of powder were introduced in a cylindrical steel container (capacity 55 ml) with two 11 mm and one 14 mm diameter steel balls. For the synthesis of Ti_2RuFe, pure Ru, Ti and Fe were used, while RuO_2 instead of Ru was used for Ti_2RuFeO_2. The container was sealed with an O-ring under argon atmosphere in a glove box. The duration of the milling was 40 h.

2.2. *Chemical and physical analyses*

The oxygen and nitrogen contents of the powders after ball-milling were measured with a TC-136 oxygen/nitrogen detector from LECO. The nitrogen and oxygen contents when no oxide is added were less than 0.1 wt % and 1.0 wt %, respectively. So, introduction of oxygen and nitrogen by air contamination is very limited.

X-ray diffraction was performed on a PHILIPS PW3040 diffractometer with CuK_α radiation. Structural parameters were extracted from the X-ray spectra by performing Rietveld refinement analyses [14, 15] using the GSAS software [16].

Scanning electron microscopy (SEM) observations of the morphology of the electrodes were made using a Hitachi S-570 microscope operating at 15 kV. The chemical analyses were performed by energy dispersive X-ray (EDX) analysis. The samples after electrolysis were cleaned with deionized water at 70 °C for 30 min prior to analysis.

The hydrogen absorption characteristics were measured in an automated gas-titration apparatus specially designed for kinetic measurements [17]. Before analysis, 1 wt % of palladium was mixed to the alloy during one hour, using the same milling equipment. The addition of palladium was necessary to improve the hydrogen absorption kinetics.

2.3. *Electrochemical measurements*

The working electrode is a pellet made by cold pressing the powders with a load of 10 000 kg cm^{-2} using a stainless steel dye of 16 mm of diameter. The powders were pressed against a Ti support. The pellets were mounted on a glass tube with resin. The electrical contact

was made on the back of the electrode by an electrical wire with silver epoxy bonding. The geometric area of the working electrode exposed to the electrolyte is 2 cm^2. A 50 cm^2 DSA® was used as counter electrode and all potentials were measured against a saturated calomel electrode (SCE) reference, using a Luggin capillary set close to the surface of the working electrode.

The electrochemical experiments were performed in a double wall glass cell with a capacity of about one litre. All experiments were performed at the standard operating temperature of the electrolysis cells in the chlorate industry (70 °C). Long-term electrolysis tests were made using industrial electrolytic solutions. During these tests, the pH of the electrolyte was maintained at about 6.5 by regular addition of HCl 10 M. The electrolytic solution was changed periodically. The cell current and cell potential were monitored continuously. From time to time, the cathodic overpotential at -250 mA cm^{-2}, η_{250}, was measured in a synthetic solution of identical composition ($NaClO_3$: 550 g dm^{-3}, NaCl: 110 g dm^{-3}, $Na_2Cr_2O_7$: 3 g dm^{-3}, NaClO:1 g dm^{-3}, pH 6.5, $T = 70$ °C). This procedure was adopted to avoid fluctuation of the electrochemical measurements due to variations of the composition of the industrial solution. So, aging of the electrodes was performed in an industrial chlorate electrolyte but the reported data points were obtained by using well-defined and reproducible electrolyte solutions.

The current–potential measurements were performed using a SI 1287 Solartron potentiostat–galvanostat, controlled by the CorrWare software. Unless specified otherwise, the ohmic drop was determined by the current interruption technique by performing a linear regression through the data obtained by varying the current density from 50 to 250 mA cm^{-2}. Usually, five data points were collected each time. In some cases, ac impedance measurements (SI 1255 Solartron HF frequency response analyser, controlled by Zplot software) were also used to determine the ohmic drop. The overpotential for hydrogen evolution at –250 mA cm^{-2} was calculated from the electrode potential value, after correction for the ohmic drop and the reversible potential of hydrogen (–681 mV vs SCE).

3. Results

3.1. *Long-term electrolysis tests*

The variation of the overpotential at –250 mA cm^{-2} (η_{250}) of Ti_2RuFe, Ti_2RuFeO_2 and commercial steel electrodes are shown in Figure 1. In this Figure, the data refer to measurements made in the synthetic chlorate electrolyte solution. They were obtained by measuring the uncompensated resistance by the current interruption technique. Between these measurements, the electrodes were polarized continuously at –250 mA cm^{-2} in an industrial chlorate liquor.

Initially, there is no difference between the activities of Ti_2RuFe and Ti_2RuFeO_2, the η_{250} values being about

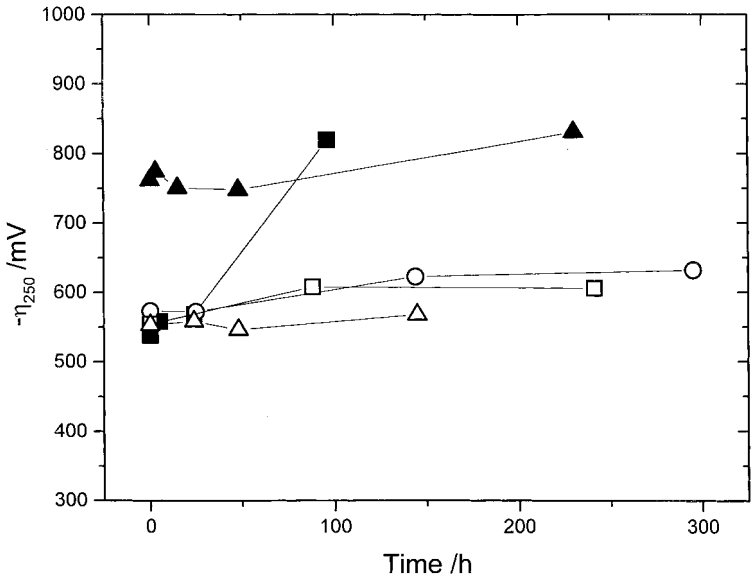

Fig. 1. Evolution of hydrogen overpotential with time at -250 mA cm^{-2} in chlorate electrolysis conditions for Ti_2RuFe, Ti_2RuFeO_2 and commercial chlorate cathode material (or alloy) supplied by Kvaerner Chemetics. Key: (■) Ti_2RuFe; (○) Ti_2RuFeO_2 (1); (□) Ti_2RuFeO_2 (2); (△) Ti_2RuFeO_2 (3); (▲) commercial electrode.

–550 mV in both cases. These results are consistent with those published previously [18], showing that the cathodic overpotential of the material does not change with the oxygen content for [O] varying from 1 to 13.6 wt %. However, the overpotential of Ti_2RuFe increases significantly after less than 100 h of electrolysis. In comparison, the overpotential recorded on Ti_2RuFeO_2 stays almost constant for about 300 h of electrolysis, the longest test performed in this study. The same nanocrystalline alloy was used in a 1000 h electrolysis test in a previous report without showing any decrease of performance [7]. The cathodic overpotential of Ti_2RuFeO_2 in chlorate electrolysis conditions is at least 200 mV lower than that of a commercial chlorate cathode material (or alloy) supplied by Kvaerner Chemetics. As shown elsewhere [11], the presence of Ru is essential for the activity of the electrode. Also, as will be seen later (Fig. 5), the surface of the cold-pressed electrode is not uniform and the electrochemically active area certainly exceeds the geometric surface of the electrode. There is no question that both factors are important in getting an active electrode for HER in chlorate liquor.

3.2. *Alternating OCP/hydrogen discharge conditions*

In the previous measurements, the electrode is brought to open circuit potential each time it is transferred from the industrial to the synthetic chlorate liquor. If corrosion or oxidation occurs at open-circuit potential (OCP), the alternating hydrogen discharge and oxidation conditions could play a significant role in the degradation of electrodes.

Three different experiments were performed on freshly prepared electrodes to investigate these effects. In the first one (A), the electrode was galvanostatically (-250 mA cm^{-2}) polarized immediately after its immersion in the chlorate electrolyte. In the second one (B), the electrode was left at open circuit potential in the electrolyte (70 °C) during 4 h before being galvanostatically polarized (-250 mA cm^{-2}). In the experiment (C), the electrodes were subjected to an alternating sequence of OCP (10 min) and galvanostatic polarization (-250 mA cm^{-2}) (10 min). In each of these experiments, the ohmic drop was determined by ac impedance measurements.

The variation of η_{250} of Ti_2RuFe electrodes in time for experiments A, B and C described above is given in Figure 2. In A, there is no variation of the overpotential of Ti_2RuFe over a 4 h period of continuous electrolysis. Likewise, the η_{250} value of Ti_2RuFe, after having been 4 h in open circuit potential in the electrolyte, does not vary much over the same period of time (B). However, it is worth noticing that the electroactivity of the electrode in B is larger (smaller η_{250} value) than that in A ($\eta_{250} = -560$ mV as against -590 mV).

The variation of η_{250} of Ti_2RuFe in experiment C is drastically different from the two previous cases. After

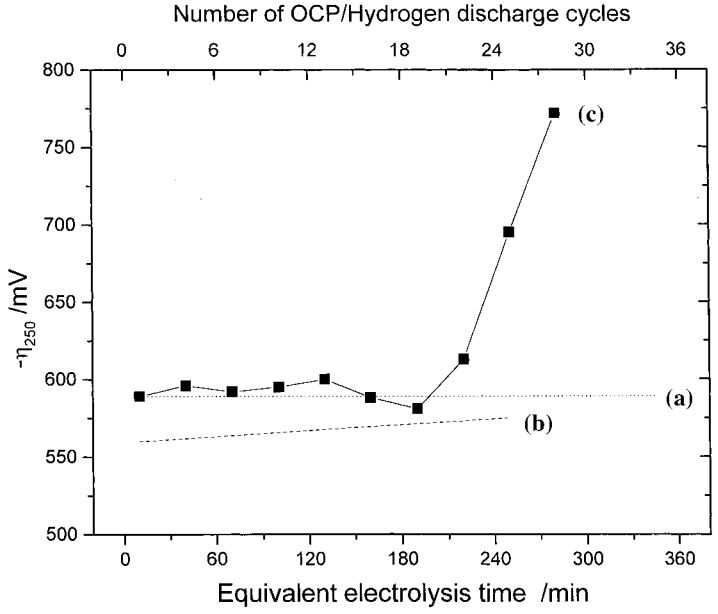

Fig. 2. Evolution of η_{250} with equivalent time of electrolysis for Ti_2RuFe electrodes: immediately after immersion in the chlorate electrolyte (a), after 4 h at open circuit condition (b), and through a succession of OCP and hydrogen discharge cycles (c). Key: (a: ·····) hydrogen discharge; (b: - - - -) hydrogen discharge after OCP; (c: ■) OCP/hydrogen discharge cycles.

190 min of electrolysis (19 cycles of OCP/hydrogen discharge), the η_{250} value decreases and reaches −775 mV after 280 min. During the degradation, significant amount of nanocrystalline powder leaves the surface of the electrode and the uncompensated resistance increases from 0.2 to 0.35 Ω. After completion of the test, parts of the electrode have lost their blackish coloration to adopt a grayish appearance. Obviously, the conditions of test C are far more stringent than those of tests A and B.

The variation of η_{250} as a function of the number of OCP/hydrogen discharge cycles was also measured on Ti_2RuFeO_2 and is compared to Ti_2RuFe in Figure 3. In the case of Ti_2RuFeO_2, about 30 cycles were made without seeing any appreciable variation of the cathodic overpotential. A visual inspection of the electrode surface after this experiment does not reveal any sign of degradation. Thus, Ti_2RuFeO_2 is much less sensitive to OCP/hydrogen discharge cycles than the oxygen free alloy. These results are consistent with the performances observed during long-term electrolysis (see Fig. 1).

3.3. *OCP evolution after strong hydrogen discharge*

The variation of the open circuit potential with time of Ti_2RuFe and Ti_2RuFeO_2 electrodes following periods of hydrogen discharge of experiment C are given after various number of cycles in Figure 4(a) and (b), respectively. For clarity, only the most representative curves are drawn. In the case of Ti_2RuFeO_2, all curves have a similar shape. At the beginning, the OCP increases slowly with time. Then, there is a change of slope in the curves. This change occurs at about 40, 75 and 180 s for the 1st, 5th and 28th curves, respectively. During this initial period, hydrogen evolution at the electrode is clearly discernable, even if the current has been switched off. The fact that hydrogen evolution continues long after that the current has been switched off helps to maintain a larger pH value in the vicinity of the electrode. The change of slope is most probably related to the fact that the pH in the vicinity of the electrode decreases slowly to reach the value in the bulk of the electrolyte (pH 6.5) when hydrogen evolution stops.

In the case of Ti_2RuFe, the curves taken after the first and the fifth cycle exhibit all the characteristic features of those of Ti_2RuFeO_2, namely, the OCP value increases slowly after switching off the current, with concomitant hydrogen evolution for 85 and 180 s, respectively. However, the time evolution of the OCP of Ti_2RuFe after cycle number 28 is radically different from the previous two. In particular, the slow decrease of the OCP value is not observed. This curve most closely resembles that recorded on a Ti electrode taken in similar conditions (see Fig. 4).

3.4. *Morphological and chemical analyses*

The SEM micrographs of Ti_2RuFe before and after prolonged hydrogen evolution (96 h) at –250 mA cm^{-2} are shown in Figure 5(a) and (b), respectively. Before

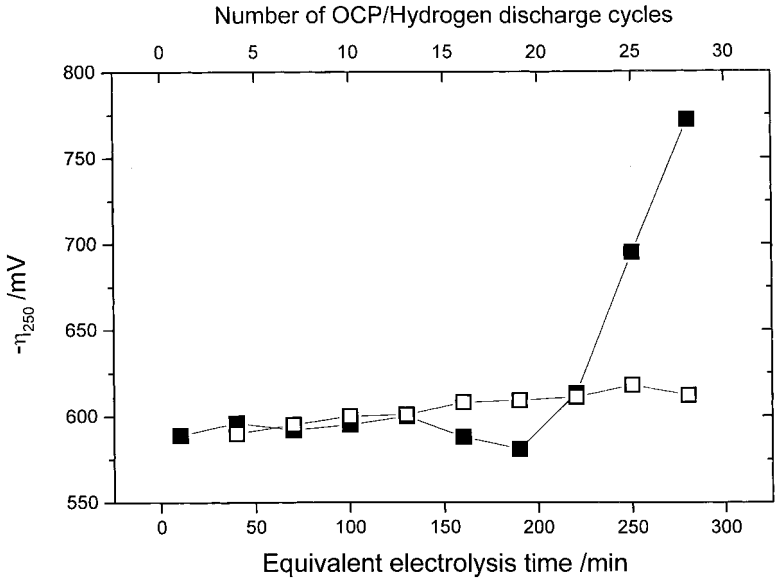

Fig. 3. Evolution of overpotential for HER at –250 mA cm^{-2} as a function of equivalent electrolysis time after successive cycles involving 10 min of open circuit and 10 min of hydrogen discharge. Key: (■) Ti_2RuFe; (□) Ti_2RuFeO_2.

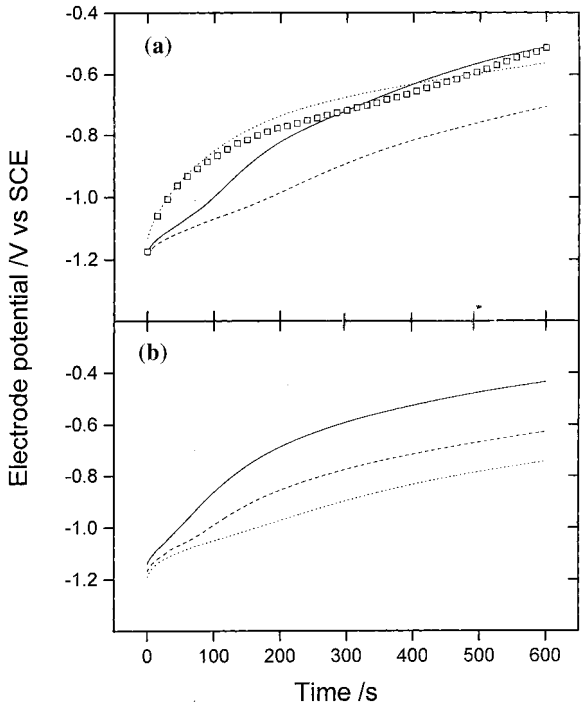

Fig. 4. Evolution of open circuit potential after hydrogen discharge (10 min, –250 mA cm^{-2}) for Ti_2RuFe (a) and Ti_2RuFeO_2 (b). OCP evolution of a Ti electrode in similar conditions is also shown. Key: (—) 1st; (- - - -) 5th; (· · · · ·) 28th; (□) titanium.

electrolysis, numerous small particles are visible at the surface of the electrode (Figure (a)). After 96 h of electrolysis, these particles are no longer observed. These morphological changes are accompanied by a variation of the chemical composition of the electrode surface. As shown in Table 1, the composition of the electrode before electrolysis is close to that expected from the nominal composition of the powder mixture. An enrichment in Fe can, however, be noticed, most probably attributable to the erosion of the steel balls and container during the milling process.

After prolonged H_2 discharge, Ti is almost exclusively found at the surface of the electrode. This Ti originates from the titanium support on which the nanocrystalline powder was pressed. This indicates that the electrocatalytic layer has been removed from the substrate after prolonged electrolysis.

The SEM micrographs of Ti_2RuFeO_2 before and after prolonged H_2 evolution (300 h) at –250 mA cm^{-2} are shown in Figure 5(c) and (d), respectively. The surface morphologies of these two electrodes are similar. Moreover, the chemical composition of Ti_2RuFeO_2 after prolonged electrolysis is close to the initial composition. The presence of chromium, probably under the form of oxides (Cr_2O_3) and/or hydroxides ($Cr(OH)_3$) [19, 20] is also detected. It originates from the reduction of dichromate at the surface of the electrode during HER.

3.5. *Hydrogen absorption properties*

The gas phase hydrogen absorption properties of Ti_2RuFe and Ti_2RuFeO_2were determined by exposing the nanocrystalline materials to hydrogen at high pressure (1.2 MPa). In both cases, a small amount (1.0 wt %) of catalyst (Pd) was added to increase the kinetics of the reaction. The results are given in Figure 6, where the hydrogen content, expressed as the number of hydrogen atom absorbed per metal atom (H/M), is displayed as a function of time. There is no hydrogen absorption in Ti_2RuFeO_2. On the other hand, hydrogen is readily absorbed in Ti_2RuFe. The maximum hydrogen content is close to $H/M = 0.12$. This corresponds to a stoichiometry close to $Ti_2RuFeH_{0.5}$.

4. Discussion

The experiment (b) of Figure 2 reveals that oxidation alone of Ti_2RuFe under open-circuit conditions do not produce degradation of the electrocatalytic layer as observed in Figure 5(b). Indeed, leaving Ti_2RuFe in open-circuit conditions before the application of a cathodic potential causes an increase of the electrode activity (compare (a) and (b) in Figure 2). This improvement could arise from a selective corrosion process leading to a Ru enrichment at the surface. However, additional experiments need to be performed to confirm this issue. Likewise, hydrogen evolution alone do not generate severe degradations (curve (a) of Figure 2). It is the combination of both (hydrogen discharge and open-circuit conditions) that causes the deterioration.

At first glance, it may seem odd that the Ti_2RuFe electrode of Figure 1 falls apart after roughly 100 h of continuous electrolysis while it does not withstand more than a few hours of equivalent time of electrolysis in curve (c) of Figure 2. However, it must be remembered that the ohmic resistance in Figure 1 was recorded by the current interruption technique, through the application of five current values. Since the electrode is brought to open-circuit conditions between each application of current, these measurements are similar to those made in experiment (c) of Figure 2 (OCP/hydrogen discharge cycles), but the frequency of current interruption is less in Figure 1. Therefore, it seems that the determining factor in the long-term electrolysis test is not so much the duration of the electrolysis, but the fact that the cathodic polarization is interrupted from

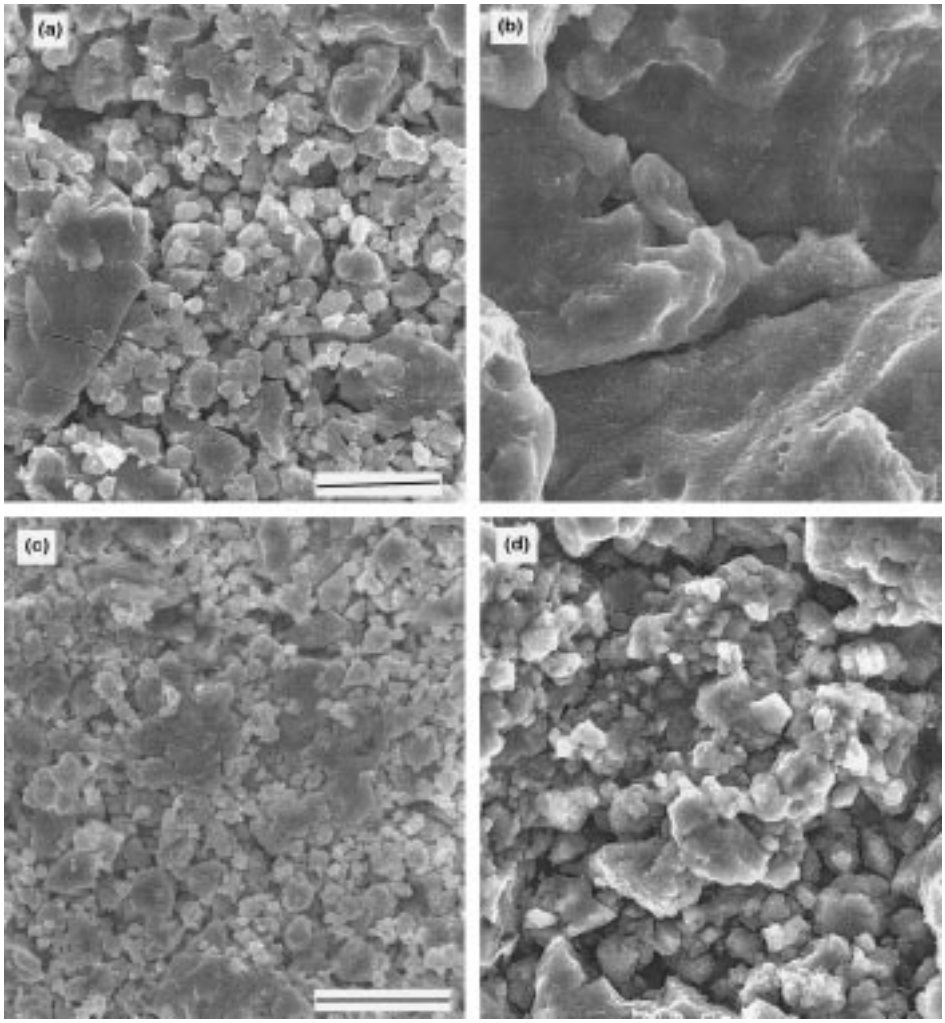

Fig. 5. SEM micrographs before (a) and (c) and after (b) and (d) prolonged electrolysis at -250 mA cm^{-2} in chlorate electrolyte: (a) and (b): Ti_2RuFe; (c) and (d): Ti_2RuFeO_2. Scale bars: 6 μm.

time to time. The same mechanism is at the origin of these results.

It has been shown in a previous report that, after hydrogen discharge in NaOH, the open circuit potential of nanocrystalline Ti_2RuFe stays cathodic of the reversible hydrogen potential for long periods of time after switching off the current [12]. As described elsewhere, [12, 21, 22], this suggests that a process different from

Table 1. Chemical analyses of Ti_2RuFe and Ti_2RuFeO_2 electrodes before and after prolonged hydrogen discharge at -250 mA cm^{-2} in chlorate electrolysis conditions

Electrode	Ti /at. %	Ru /at. %	Fe /at. %	Cr /at. %	Na /at. %
Ti_2RuFe before H_2 discharge	43	22	35	–	–
Ti_2RuFe after prolonged H_2 discharge (96 h)	98	0	1	1	0
Ti_2RuFeO_2 before H_2 discharge	49	26	25	–	–
Ti_2RuFeO_2 after prolonged H_2 discharge (295 h)	45	29	19	5	2

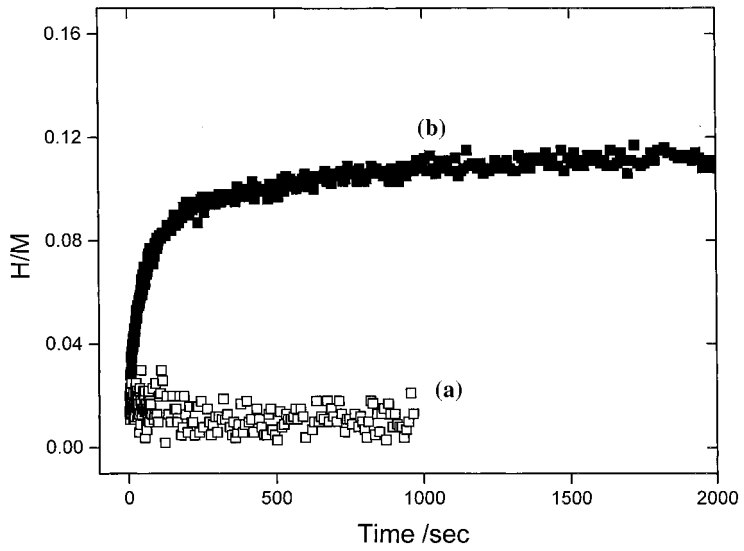

Fig. 6. Gas phase hydrogen absorption curves of (a) Ti_2RuFeO_2 and (b) Ti_2RuFe. In both cases, 1 wt % of Pd was added to the powder to catalyse the decomposition of H_2 into atomic hydrogen. Measurements performed at room temperature and at 1.2 MPa.

the reversible H_2/H_2O reaction, with a redox potential changing in time, occurs at the electrode. In NaOH, this process is related to the formation of an hydride and its decomposition at open-circuit conditions. Figure 6 confirms that nanocrystalline Ti_2RuFe readily absorbs hydrogen. Thus, following hydride formation under hydrogen discharge, a self-discharge process is expected to take place through a mixed mechanism where anodic hydride decomposition is coupled concurrently with cathodic hydrogen evolution. In the case of Ti_2RuFe in NaOH, the two basic parallel reactions are:

$$Ti_2RuFeH_x + xOH^- \rightarrow Ti_2RuFe + xH_2O + xe^-(\text{anodic}) \quad (1)$$

$$H_2O + e^- \rightarrow OH^- + 1/2H_2 \quad (\text{cathodic}) \quad (2)$$

In open circuit, the above anodic and cathodic reactions are coupled as in a corrosion process, with the net decomposition of Ti_2RuFeH_x taking place at a mixed potential, E_M. The potential E_M is determined by the potential of the more reversible of the two coupled processes, that is, the equilibrium potential for anodic hydride decomposition [21]. Therefore, the equilibrium potential of Reaction 1 can be considered as equal to E_M and will depend on the hydrogen content in the alloy. The slow variation of the OCP observed after subjecting the electrode to a hydrogen discharge in NaOH reflects the continuous decrease of the amount of H in the alloy.

Obviously, the fact that Ti_2RuFe is able to form an hydride in NaOH under hydrogen discharge does not mean that the same holds true in the chlorate electrolyte. It is indeed well known that a chromium hydroxide layer forms on the surface of cathodes in chlorate electrolyte [19, 20] and its presence may affect hydride formation. However, Figure 4 shows that the open-circuit potential of Ti_2RuFe varies slowly over a period of several seconds after current interruption. During that period, hydrogen gas is evolved continuously from the electrode surface. These results suggest that hydrides also form in chlorate electrolyte. The duration of the slow variation of OCP increases from the first to the fifth cycle suggesting that the amount of hydride formed increases with the number of cycles [23]. The curve after the 28th cycle behaves differently because the electrocatalytic layer at that point has been destroyed (see Figs 2 and 4). The degradation of Ti_2RuFe is most probably related to the change in volume associated with the hydrogenation/de-hydrogenation cycles which take place when the electrode is successively polarized cathodically and left in open-circuit conditions.

Two hypotheses can be proposed to explain the improved stability of the O containing nanocrystalline electrode. These are as follows:

(i) stabilization effect due to the presence of extraneous phases and thin oxide layers. The X-ray and neutron diffraction patterns of nanocrystalline Ti_2RuFe and Ti_2RuFeO_2 have been shown elsewhere [10, 24, 25] and the structural data obtained from Rietveld refinement analysis of these diagrams are given in Table 2. The nanocrystalline Ti_2RuFe alloy is made almost exclusively (>97 wt %) of a cubic phase (cP2, CsCl), with only a small proportion (<3 wt %) of iron. The lattice parameter of the B2 structure is

Table 2. Structural parameters of the milled powders obtained from the Rietveld refinement analysis of the corresponding X-ray diffraction patterns

Stoichiometry	Phase identification	Lattice parameters		Crystallite size /nm	Phase concentration /wt %
		a/pm	*c*/pm		
Ti_2RuFe	Ti_2RuFe	303.1		7	97.3
	Fe	287.3		11	2.7
Ti_2RuFeO_2	Ti_2RuFe	302.9		10	58.8
	TiO_x	412.6		28	31.3
	Ru	270.9	421.9	35	9.9

303.1 pm which is close to the mean value between FeTi (296.0 pm) and RuTi (306.0 pm) [10]. On the other hand, nanocrystalline Ti_2RuFeO_2 is made of several phases including the B2 structure (58.8 wt %), titanium oxide (31.3 wt %), and Ru (9.9 wt %). It is well known that thin oxide coatings on metals can prevent hydrogen uptake [26]. For example, several studies have demonstrated that titanium oxides act as a barrier to hydrogen penetration [27, 28]. As shown in Table 2, Ti_2RuFeO_2 contains more that 30 wt % of titanium oxide, which can act to retard or hinder hydride formation. At the first glance, this seems to be confirmed by the results of Figure 6, showing that hydrogen from the gas phase is not absorbed by Ti_2RuFeO_2. However, the variation of the OCP with time after the current has been switched off (Figure 4) is indicative of the fact that an hydride is formed. This is consistent with our most recent results on the behavior of Ti_2RuFeO_2 in NaOH, suggesting that an hydride is formed under hydrogen discharge conditions although to a lesser extent than in Ti_2RuFe [23]. Therefore, it is not evident that the titanium oxide phase formed during the milling operation of Ti–Ru–Fe in presence of O acts as an effective protection against hydride formation of the B2 structure during electrolytic hydrogen discharge. Modification (reduction of the titanium oxide phase during hydrogen discharge could explain why Ti_2RuFeO_2 is able to absorb hydrogen in solution and not in the gas phase.

(ii) Modification of the hydrogen absorption properties of the cubic phase due to Ti depletion in the B2 structure [25]. When x in Ti_2RuFeO_x increases from 0 to 1.5, the stoichiometry of the B2 structure changes from Ti_2RuFe to $Ti_{1.26}Ru_{1.2}Fe_{1.5}$. The decrease of the Ti content should reduce the hydrogen absorption capacity of the B2 structure.

At this time, it is difficult to confirm which of these hypotheses is valid or if both play a role. More experiments will be requested to resolve this issue.

5. Conclusion

It was shown that the nanocrystalline Ti_2RuFe electrode suffers from severe decrepitation when it is subjected to alternate cycles of hydrogen discharge and open circuit conditions. This arises as a result of hydrogen absorption and desorption. Most probably, the volume expansion associated with hydride formation and the volume contraction occurring during hydrogen desorption induces stresses in the electrode and the decrepitation of the material. An accelerated ageing test to assess the long-term stability of nanocrystalline Ti_2RuFe has been devised, whereby the electrode is subjected to a series of alternating cycles of hydrogen discharge and open circuit conditions.

It has also been shown that the presence of oxygen in the alloy is crucial for the long-term stability. In the case of Ti_2RuFeO_2, up to 300 h of continuous electrolysis tests and up to 30 OCP/hydrogen discharge cycles have been completed without any sign of deterioration of the electrode. The beneficial effect of O could be due to: (i) the presence of oxide phases in particular titanium oxide, and (ii) the depletion of Ti from the cubic phase which reduces hydrogen absorption. Obviously, more prolonged OCP/electrolysis cycles or longer electrolysis tests will have to be realized on these electrodes to meet the requirements of the industry.

Acknowledgements

This work has been financially supported by Hydro-Québec and the National Sciences and Engineering Research Council (NSERC) of Canada, through a University – Industry grant. We would also like to thank Kvaerner Chemetics for supplying a commercial chlorate cathode material (or alloy).

References

1. K. Viswanathan and B.V. Tilak, *J. Electrochem. Soc.* **131** (1984) 1551.

2. S. Trasatti, *in* 'Advances in Electrochemical Science and Engineering', vol. 2, edited by H. Gerischer and C.W. Tobias (VCH, New York, 1990) p. 1.
3. R. Schulz, J.Y. Huot, M.L. Trudeau, L. Dignard-Bailey, Z.H. Yan, S. Jin, A. Lamarre, E. Ghali, A. Van Neste, *J. Mater. Res.* **9** (1994) 2998.
4. C. Suryanarayana, *in* 'Bibliography on Mechanical Alloying and Milling' (Cambridge Interscience, Cambridge, UK, 1995).
5. C.C. Koch and J.D. Whittenberger, *Intermetallics* **4** (1996) 339.
6. 'Alliages à base de Ti, Ru, Fe et O et usages de ceux-ci pour la fabrication de cathodes pour la synthèse électrochimique du chlorate de sodium'. Ref. 27881-0465, Patent pending.
7. A. Van Neste, S. Jin, S.H. Yip, D. Guay, S. Boily and R. Schulz, *Mater. Sci. Forum* **2250–227** (1996) 795.
8. M. Blouin, D. Guay, S. Boily, A. Van Neste and R. Schulz, *Mater. Sci. Forum* **225–227** (1996) 801.
9. M. Blouin, L.Roué, S.H. Yip, D. Guay, J. Huot, S. Boily, A. Van Neste and R. Schulz, *Mater. Sci. Forum* **235–238** (1997) 979.
10. M. Blouin, D. Guay, J. Huot and R. Schulz, *J. Mater. Res.* **12** (1997) 1492.
11. S.H. Yip, D. Guay, S. Jin, E. Ghali, A. Van Neste and R. Schulz, *J. Mater. Res.* **13** (1998) 1171.
12. L. Roué, D. Guay and R. Schulz, *J. Electroanal. Chem.* **455** (1998) 83.
13. J.O'M. Bockris and A.K.N. Reddy, *in* 'Modern Electrochemistry', vol. 2 (Plenum Press, New York, 1970), chapter 11.
14. F. Izumi, *in* 'The Rietveld Method', edited by R.A. Young (Oxford University Press, Oxford, 1993), pp. 236–253.
15. R.B. Von Dreele, *in* 'The Rietveld Method', edited by R.A. Young (Oxford University Press, Oxford, 1993), pp. 227–235.
16. A.C. Larson and R.B. Von Dreele, 'GSAS-General Structure Analysis System', Los Alamos National Laboratory Report LA-UR 86-748 (1986).
17. 'Appareil pour la titration des gaz et le cyclage des matériaux absorbants et adsorbants', Canadian patent pending 2.207.149.
18. M. Blouin, D. Guay and R. Schulz, *Nanostructured Materials* **10** (1998) 523.
19. B.V. Tilak, K. Viswanathan and C.G. Rader, *J. Electrochem. Soc.* **128** (1981) 1228.
20. Ahlberg Tidblad and J. Martensson, *Electrochim. Acta.* **42** (1997) 389.
21. B.E. Conway, H. Angerstein-Kozlowska, M.A. Sattar, B.V. Tilak, *J. Electrochem. Soc.* **130** (1983) 1825.
22. L. Vracar and B.E. Conway, *J. Electroanal. Chem.* **277** (1990) 253.
23. L. Roué, D. Guay and R. Schulz, in preparation.
24. M. Blouin, D. Guay, R. Schulz, submitted to *J. Mater. Sci.*
25. M. Blouin, D. Guay, J. Huot, R. Schulz and I.P. Swainson, *Chem. Mater.* **10** (1998) 3492.
26. G.T. Murray, *in* 'Prevention of Hydrogen Embrittlement by Surface Films – Hydrogen Embrittlement: Prevention and Control', edited by L. Raymond (American Society for Testing and Materials, Philadelphia, 1988), p. 304.
27. L.C. Covington, *Corrosion* **35** (1979) 378.
28. R.W. Shultz and L.C. Covington, *Corrosion* **37** (1981) 585.